

Rayleigh-Taylor Instability in Elastic-Plastic Materials

Guy Dimonte,¹ Robert Gore,² and Marilyn Schneider¹

¹Lawrence Livermore National Laboratory, Livermore, California 94551

²Los Alamos National Laboratory, Los Alamos, New Mexico 87545

(Received 23 July 1997)

The Rayleigh-Taylor instability is investigated in a material with a shear modulus μ and yield stress σ_0 . Incompressible experiments are conducted with constant and impulsive acceleration histories $g(t)$ using a fully characterized material. Two dimensional (2D) perturbations are found to be stabilized for wave number $k > \rho g/2\mu$ and initial amplitude $h_0 < \sigma_0/\rho g$, where ρ is the density. The stability region is larger for 3D perturbations. Unstable modes are found to grow classically during the acceleration phase, but they can recover elastically while coasting. [S0031-9007(97)05230-7]

PACS numbers: 47.20.Bp, 47.50.+d

When an elastic-plastic plate is accelerated by a lower density fluid, the interface between them is Rayleigh-Taylor (RT) unstable [1–7], but the mechanical strength of the plate mitigates the growth. This occurs when metal plates are accelerated by high explosives (HE) [6,8–10] or electrical currents [11], and in volcanic island formation due to the strength of the earth's crust [12].

The effect of a shear modulus μ and a tensile yield σ_0 on RT stability is reviewed nicely by Robinson and Swegle (RS) [3]. The elastic force $\sim -2\mu k^2 h$ can overcome the RT buoyancy $\sim \rho g k h$ and stabilize small amplitude ($kh \ll 1$) perturbations with wave numbers

$$k > \rho g/2\mu \equiv k_c, \quad (1)$$

where ρ is the plate density and g is the acceleration. These modes may again be destabilized if the pressure drop across the initial amplitude h_0 exceeds the yield stress and drives the plastic flow, i.e.,

$$P^* \equiv \rho g h_0/2\sigma_0 \geq P_{cr}. \quad (2)$$

Estimates of the critical scaled pressure P_{cr} for two dimensional (2D) perturbations are $\sim 1.15/(1 + e^{-kH})$ by Miles [1], where H is the plate thickness, ~ 1 by Drucker [2], $\sim 0.58[b + (b^2 + 1)^{1/2}]^{1/2}$ by RS [3], where $b \equiv 1 - e^{-2kH}$, and $\sim (1 - 0.86e^{-kH/\sqrt{3}})[(1 - e^{-kH/\sqrt{3}})^2 - (k_c/k)^2]$ by Nizovtsev and Raevskii (NR) [5,6]. The stability may be enhanced in 3D [2] with $P_{cr} \sim 2$ and reduced growth rates [6].

Experiments [6,8–10] in which metal plates are accelerated by HE find a $P_{cr} < 1$ that decreases with $\lambda \equiv 2\pi/k$ and show slower growth in 3D than in 2D [5]. Unfortunately, the uncertainties are large, $\sim 50\%$, because the parameter variations are coarse and the material properties are uncertain at the high pressure. For example, to explain the observations, it is necessary to increase the static yield tenfold for weak aluminum (1100-0) but not for strong aluminum (6061-T6) and steel. If there is a strain rate dependence, as with viscosity (η), a reduced RT growth rate [3] may appear as strength since the experiments are short $t \sim 2/\sqrt{kg}$. Also, Eq. (1) could not be tested because $\lambda_c = 2\pi/k_c$ exceeded the plate width.

Numerical simulations [4,6] can treat the nonlinear constitutive properties and complex $g(t)$ profiles. For 10 GPa drive pressures, the simulations obtain $P_{cr} \sim 0.4$ at $\lambda = 2H$ consistent with the HE experiments. However, the critical wavelength is observed to be much smaller than $4\pi\mu/\rho g$ for the experimental conditions, possibly because $k_c H \ll 1$. At higher pressures, the values of P_{cr} are orders of magnitude smaller than Eq. (2). This discrepancy can be reconciled [3,7] by replacing the unstressed initial amplitude h_0 in Eq. (2) by the new equilibrium amplitude after the drive pressure is applied. The simulations also find a strong sensitivity to the acceleration history due to the generation of elastic waves.

Here, we conduct experiments on the Linear Electric Motor (LEM) [13] using different acceleration profiles to measure the critical wavelength λ_c and amplitude P_{cr} , and to compare 2D and 3D perturbations. The elastic material is chosen to be yogurt because its constitutive properties (μ, η, σ_0) are well characterized [14] and satisfy Eqs. (1) and (2) for the accelerations obtainable on the LEM. These scaled experiments complement those at high pressure because a higher precision is possible since the constitutive properties are known and the parameters are more easily varied.

The yogurt is prepared from scratch in the test molds so that the samples are undisturbed (virgin). Yogurt is incompressible with density $\sim 1.04 \text{ g/cm}^3$. The constitutive properties were obtained at 8–10 °C using six different tests [14], some of which are exemplified in Fig. 1. A stress-strain curve for a yogurt cylinder is shown in Fig. 1(a). For unidirectional compression (solid line), we obtain $\mu = 1030 \text{ Pa}$ and $\sigma_0 \sim 280 \text{ Pa}$. For bidirectional loading (dashed line), we observe a hysteresis with an average $\mu \sim 1530 \text{ Pa}$. We corroborate the yield measurement by extruding a yogurt cylinder in earth's gravity (g_0) as shown in Fig. 1(b). The yogurt yields when its length becomes $\sigma_0/\rho g_0$, which we measure to obtain $\sigma_0 \sim 340 \text{ Pa}$. Conventional tests [14] with vane and cone-plate rheometers give a shear yield of 175 and 190 Pa, respectively, consistent with [3] $\sigma_0/\sqrt{3}$. We show unequivocally that

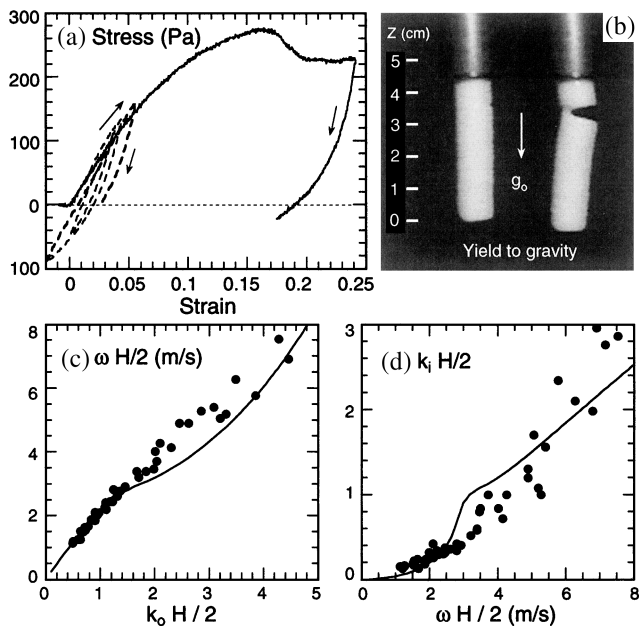


FIG. 1. (a) Stress/strain curve of the compressed yogurt cylinder. (b) Yogurt cylinder in earth's gravity with a maximum self-supporting length of $\sim \sigma_0/\rho g_0$. (c) Frequency vs wave number and (d) damping decrement of elastic waves with $H = 4$ cm. Points are measured and lines are calculated with $\mu = 1500$ Pa and $\eta = 5$ Pa.s.

$\sigma_0 \neq 0$ by inverting an open container of yogurt at g_0 with no observed motion for 10^6 s. The dynamic properties are obtained [14] from elastic waves of frequency ω . Roughly, the wave number is $k_0 \sim \omega/\sqrt{\mu/\rho}$ and the damping decrement is $k_i \sim \eta \omega^2/\sqrt{\mu^3/\rho}$. The solid points in Figs. 1(c) and 1(d) are measured for a yogurt slab of thickness $H = 4$ cm, and the lines are solutions to the full dispersion relation [14] with $\mu = 1500$ Pa and $\eta = 5$ Pa.s. This value of μ agrees with the bidirectional result in Fig. 1(a), and shows that the elastic waves sample the hysteresis. This measurement of μ and η uses a dispersion relation [3] that is applicable to the RT instability. Based on these diverse tests, the dynamic properties of yogurt are $\mu = 1500 \pm 300$ Pa, $\sigma_0 = 315 \pm 60$ Pa, and $\eta = 5 \pm 1.5$ Pa.s.

The RT experiments are conducted with virgin yogurt at 8–10 °C. The preparation starts two days prior by pouring the mixed ingredients into a test mold and placing it in the refrigerator to solidify. The mold cavity has horizontal dimensions of $W_x = 6$ cm by $W_y = 6.3$ cm and a height $H \sim 3.2$ cm. Initially, we overfill the mold to $H \sim 5$ cm to aid the cutting of the sinusoidal perturbations. Just before an experiment, they are cut with a thin taut wire at the top of the mold using patterned guides and the excess is removed. The remaining yogurt is undisturbed and fully supported with all surfaces flush with the mold walls. Thus, for 2D perturbations, the patterns are also in the front and back mold walls. For 3D tests, the mold walls are flat and the patterns are first

cut sideways as in 2D and then trimmed front to back using guides at the side. The yogurt filled mold is then sealed into the projectile. The light accelerating fluid is N_2 pressurized to $2.3 \cdot 10^5$ Pa, which is much greater than the dynamic pressure, $\rho g H \sim 10^4$ Pa, so that the nitrogen remains uncompressed with a density ~ 5 mg/cm³.

The yogurt is accelerated in the LEM, which has been used for RT experiments in Newtonian fluids [15]. A downward electromagnetic force is obtained in an augmented rail gun configuration with linear electrodes (rails) and sliding armatures. The power supply consists of 16 capacitor banks (450 V, 0.36 F each) which can be independently charged and discharged to vary the acceleration profile $g(t)$. The acceleration is measured with piezoresistive accelerometers. The projectile has a total mass of 1.8 kg, clear plastic windows for viewing, and a fluid cavity that is 7.3 cm wide, 7.3 cm deep, and 8.8 cm high. Stop-action pictures are taken with eight computerized electronic cameras and flash backlighters (5 μ s). Only the spikes with amplitude h_s are seen since yogurt is opaque.

The existence of a critical wavelength is shown in Fig. 2 with a flat initial interface ($h_0 < 0.1$ mm). Since only modes with $\lambda > \lambda_c = 4\pi\mu/\rho g$ should be unstable and λ is limited by the mold dimensions, the instability should appear only at high acceleration when λ_c fits into the mold. The circles in Fig. 2(a) show two different responses with a constant acceleration (dashed line) at $53g_0$ ($g_0 = 9.8$ m/s²) since this is the transitional case. The solid circles and Fig. 2(b) represent a stable case in which the amplitude increases to an equilibrium level of $h_s \sim 1$ mm due to spontaneously generated waves near the edges. The open circles and the image in Fig. 2(c) show considerable growth. In six cases with $g \leq 48g_0$, we observe stable behavior similar to that in Fig. 2(d) with edge waves of $h_s \sim 1$ mm. All cases with $g \geq 55g_0$ are unstable. Thus, the instability appears

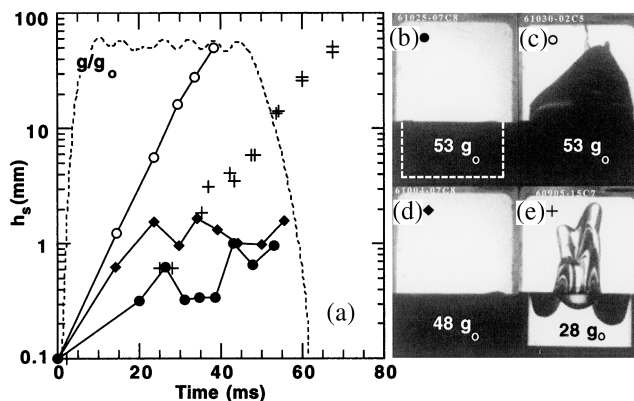


FIG. 2. (a) Spike evolution for flat initial interface, $h_0 \leq 0.1$ mm. Symbols (\bullet , \circ , \blacklozenge) and sample images [(b)–(d)] at 53, 38, 55 ms) are for yogurt and (+) and image (e) are for corn syrup. Acceleration profile (dashed line) is shown for $53g_0$, but the magnitude is varied as indicated on images.

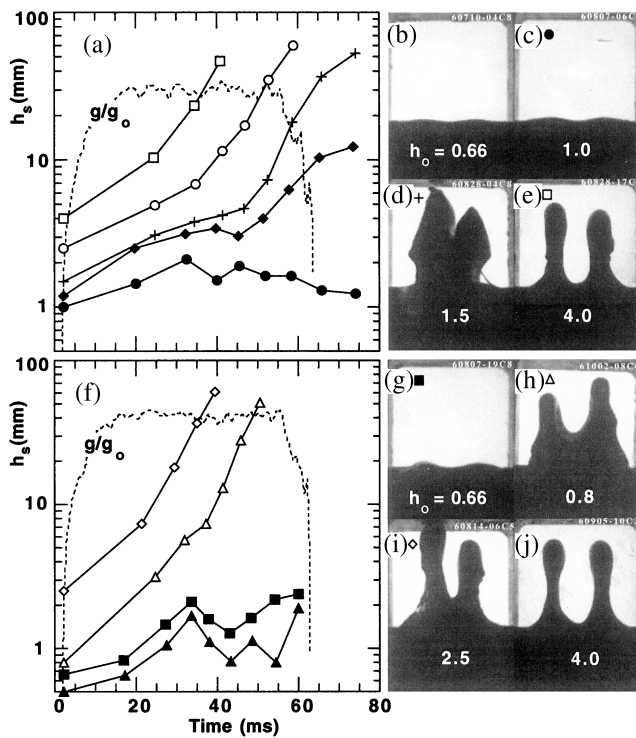


FIG. 3. Spike evolution (points) for 2D perturbations ($\lambda = 3$ cm) with (a) $g = 28g_0$ and (f) $g = 40g_0$ (dashed lines). Sample images at $t = 75, 74, 74, 41$ ms [(b)–(e)] and $t = 60, 51, 43, 34$ ms [(g)–(j)] with indicated h_0 (mm).

between 48 and $53g_0$. This is compared with Eq. (1) by setting [16] $k^2 \equiv (2\pi/W_x)^2 + (2\pi/W_y)^2 = k_c^2$ since the resultant perturbations are 3D. This predicts instability when $g \geq (43 \pm 8)g_0$ for $\mu \sim 1500 \pm 300$ Pa, which is consistent with our results. The observed stability with yogurt is not due to viscosity since experiments with corn syrup, a Newtonian fluid with a viscosity $\eta \sim 4$ Pa s similar to yogurt, are unstable even at $28g_0$ [(+) data points and Fig. 2(e)].

The critical amplitude is investigated in Fig. 3 with imposed 2D perturbations ($\lambda = 3$ cm) and a constant $g(t) \leq 40g_0$ to satisfy Eq. (1) ($k \geq 1.6k_c$) for stability. The amplitude threshold Eq. (2) is obtained by increasing h_0 as indicated at 2 ms and on the images in mm. Figure 3(a) summarizes the temporal evolution of h_s for a constant $28g_0$ (dashed line) and corresponding images are shown in Figs. 3(b)–3(e). For $h_0 = 1$ mm (●), the perturbation is stable, but it stretches elastically to a new equilibrium $h_s \sim 1.5$ mm due to the increased gravitational stress. For $h_0 = 1.2$ mm (◆), h_s increases tenfold over the shot. This is the critical amplitude since one additional shot was stable and another unstable. Strong growth is observed for $h_0 \geq 1.5$ mm, but only after a 40 ms delay time. This delay is an elastic effect and decreases with h_0 . Once unstable, the flow becomes plastic and limited by viscosity. The growth is exponential $\exp(\gamma t)$ with similar $\gamma \sim 100$ s⁻¹ for all

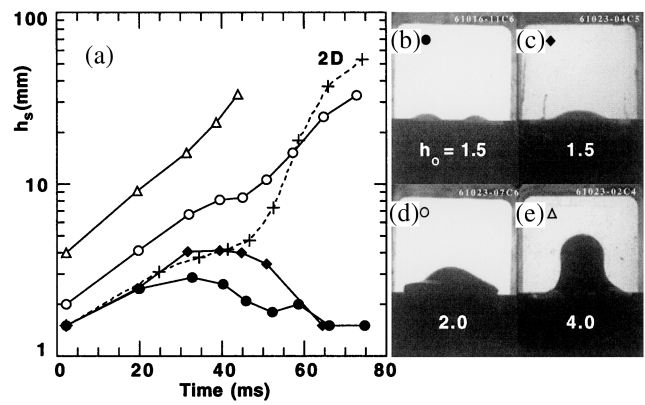


FIG. 4. (a) Spike evolution for 3D perturbations (○, ●, △, ◆) and $28g_0$. 2D perturbation (+) taken from Fig. 3(a). Wavelengths are $2\pi/k_x = 3$ (b) and 6 [(c)–(e)] cm across and $2\pi/k_y = 6.3$ cm into paper. Sample images at $t = 58, 51, 57,$ and 44 ms with indicated h_0 (mm).

$h_0 \geq 1.5$ mm. A similar growth rate is observed for corn syrup in Fig. 2 with $h_0 \sim 0$. These growth rates are 40% of classical $\sqrt{kg} \sim 250$ s⁻¹, but in agreement with linear theory [3] with viscosity ($\eta \sim 5$ Pa s), namely, $\gamma_\eta \sim 0.4(\rho g^2/\eta)^{1/3} \sim 100$ s⁻¹. This is near the peak growth rate since $k \sim (\rho\sqrt{g}/\eta)^{2/3}$. As expected at $40g_0$, Figs. 3(f)–3(j) show that the instability appears at a smaller amplitude, $0.66 < h_0$ (mm) < 0.8 , and with larger growth rates $\gamma \sim 150$ s⁻¹ $\sim \gamma_\eta$ for $h_0 \geq 0.8$ mm. The elastic stretching and time delay are also evident. For $h_0 = 4$ mm, the spikes grow robustly and develop slender bodies with enlarged tips.

Figure 4 shows that 3D perturbations are more stable than those in 2D by comparing them at $28g_0$. For $h_0 = 1.5$ mm, the perturbations are stable in 3D (●) and unstable in 2D (+). The wave number is $k \sim 2.32$ /cm in 3D ($2\pi/k_x = 3$ cm, $2\pi/k_y \sim 6.3$ cm) and 2.1/cm in 2D ($k_y = 0$). Since P_{cr} may increase [1,3,5] with k , the 3D experiments are repeated at $k \sim 1.5$ /cm ($2\pi/k_x \sim 2\pi/k_y \sim 6$ cm) in Figs. 4(c)–4(e). These 3D

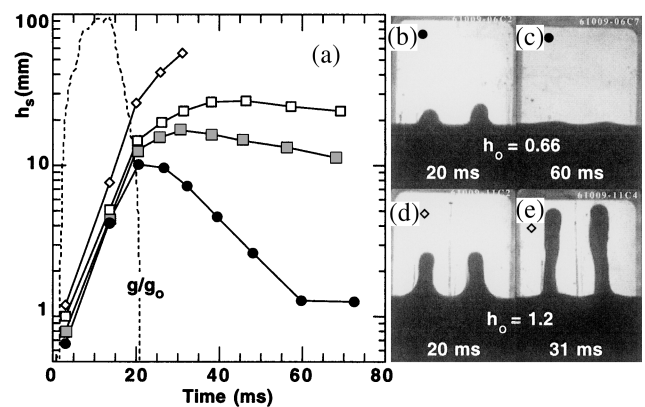


FIG. 5. (a) Spike evolution (points) for impulsive acceleration at $95g_0$ (dashed line) and 2D perturbations ($\lambda = 3$ cm). (b)–(e): Sample images with indicated time and h_0 (mm).

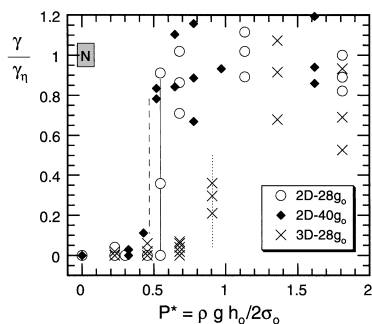


FIG. 6. Measured growth rate vs $P^* \equiv \rho g h_0 / 2\sigma_0$ for different conditions as indicated. The linear growth rate with viscosity [3] is $\gamma_\eta \sim 0.4(\rho g^2/\eta)^{1/3}$. Corn syrup (*N*) shows no instability threshold.

perturbations are also stable for $h_0 = 1.5$ mm (\blacklozenge). For $h_0 = 2$ mm, the 3D modes are only marginally unstable with a growth rate $\gamma \sim 35$ s $^{-1}$ which is smaller than that from fluid theory $\gamma_\eta \sim 105$ s $^{-1}$ and for 2D perturbations $\gamma \sim 100$ s $^{-1}$ with $h_0 = 2$ mm. The latter growth rates are attained in 3D for $h_0 \geq 4$ mm.

The elastic response of yogurt is dramatized in Fig. 5 with $\lambda = 3$ cm (2D) and an impulsive $g(t) \sim 95g_0$ (dashed line). During the acceleration, all cases are unstable since $k = 0.66k_c$ and the measured growth rate is $\gamma \sim 200$ s $^{-1} \sim \gamma_\eta$. However, for $h_0 = 0.66$ mm, the spikes recover fully during the coast phase after reaching $h_s \sim 10$ mm at 20 ms [Figs. 5(b) and 5(c)]. This is remarkable since the strain $h_s/H \sim h_s/\lambda \sim 30\%$ is larger than observed at yield in static tests [Fig. 1(a)]. For $h_0 = 0.8$ and 1 mm, the spike grows marginally into the plastic region and recovers only slightly while coasting. For $h_0 = 1.5$ mm, the spike has reached the fully plastic region to $h_s = 25$ mm at 20 ms [Fig. 5(d)] and then continues to grow during the coast phase [Fig. 5(e)]. The elastic recovery is evident but less dramatic with a constant g and it is observed in simulations [4] with elastic media.

The amplitude transition for $k > k_c$ is summarized in Fig. 6 by plotting the scaled growth rate vs P^* for constant $g(t)$. The instability appears when $P^* > P_{cr}$ with a growth rate that is within 20% of the linear rate [3] with viscosity γ_η . For 2D and $28g_0$, the threshold is $h_0 \sim 1.2$ mm, corresponding to $P_{cr} \sim 0.54$ as indicated by the solid line. For $40g_0$, the threshold is between $h_0 \sim 0.66$ and 0.8 mm, corresponding to $P_{cr} \sim 0.43$ – 0.52 . The dashed line is the average $P_{cr} \sim 0.48$. In 3D, the transition occurs at $h_0 \sim 2$ mm, corresponding to $P_{cr} \sim 0.89$ as indicated by the dotted line. This is definitely more stable than in 2D since there are six points at $P^* \sim 0.69$ with $\gamma \sim 0$. There is an uncertainty $\delta P_{cr} \sim \pm 0.1$ due to the 20% error in σ_0 , but the relative values are more precise. The Newtonian fluid (*N*, corn syrup) has a similar η and growth rate, but no amplitude threshold.

These thresholds are smaller than obtained by the models: $P_{cr} = 1.15$ by Miles [1], $P_{cr} = 0.9$ by RS [3], and $P_{cr} = 0.75$ and 0.55 for $28g_0$ and $40g_0$, respectively, by NR [5]. Drucker [2] estimates $P_{cr} = 1$ in 2D and $P_{cr} = 2$ in 3D. Thus, the model of NR [5,6] agrees best with the experiments. However, please note that the models consider a free plate, whereas the yogurt is supported by the mold, and this may be important since $\lambda \sim H$.

In conclusion, RT experiments with a fully characterized elastic-plastic material confirm Eqs. (1) and (2). Modes with $k > k_c$ are found to be stable when $\rho g h_0 / 2\sigma_0 < P_{cr} \sim 0.5$ in 2D and ~ 0.9 in 3D. This agrees best with the 2D model of NR [5] and supports the stability enhancement in 3D estimated by Drucker [2]. The elastic behavior is dramatized with an impulsive $g(t)$ in which large perturbations with $P^* \sim 3P_{cr}$ grow during the acceleration, but then recover elastically afterwards.

We thank Don Nelson and Sam Weaver for their excellent technical assistance and Dr. A. C. Robinson, Dr. S. M. Bakhrakh, Dr. V. A. Raevskii, and Dr. A. I. Lebedev for enlightening conversations. This work was performed under the auspices of the U.S. Department of Energy by the Lawrence Livermore National Laboratory under Contract No. W-7405-ENG-48 and by the Los Alamos National Laboratory under Contract No. W-7405-ENG-36.

-
- [1] J. W. Miles, General Dynamics Report No. GAMD-7335, AD643161, 1966 (unpublished).
 - [2] D. C. Drucker, *Mechanics Today*, edited by S. Nemat-Nasser (Pergamon, Oxford, 1980), Vol. 5, p. 37.
 - [3] A. C. Robinson and J. W. Swegle, *J. Appl. Phys.* **66**, 2859 (1989).
 - [4] J. W. Swegle and A. C. Robinson, *J. Appl. Phys.* **66**, 2838 (1989).
 - [5] P. N. Nizovtsev and V. A. Raevskii, *VANT Ser. Teor. Prikl. Fiz. No. 3*, 11 (1991) (in Russian).
 - [6] A comprehensive (in English) review of the Russian work can be seen in S. M. Bakhrakh *et al.*, LLNL Report No. UCRL-CR-126710.
 - [7] E. L. Ruden and D. E. Bell, *J. Appl. Phys.* **82**, 163 (1997).
 - [8] John F. Barnes *et al.*, *J. Appl. Phys.* **45**, 727 (1974).
 - [9] John F. Barnes *et al.*, *J. Appl. Phys.* **51**, 4678 (1980).
 - [10] A. I. Lebedev *et al.*, *Phys.-Dokl.* **41**, 328 (1996).
 - [11] J. Degnan *et al.*, *Phys. Rev. Lett.* **74**, 98 (1995).
 - [12] B. D. Marsh, *J. Geol.* **87**, 687 (1979).
 - [13] Guy Dimonte *et al.*, *Rev. Sci. Instrum.* **67**, 302 (1996).
 - [14] Guy Dimonte *et al.*, LLNL Report No. UCRL-JC-127477 [J. Rheol. (to be published)].
 - [15] Guy Dimonte *et al.*, *Phys. Rev. E* **54**, 3740 (1996).
 - [16] S. M. Bakhrakh and V. A. Raevskii (private communication).